The Astrophysical Journal Letters, 915:L1 (7pp), 2021 July 1 https://doi.org/10.3847/2041-8213/ac0726

Broken Power-law Energy Spectra of the Accelerated Electrons Detected in Radio and Hard X-Rays during the SOL2013-05-13 Event

Douglas Félix da Silva[1,2] and Adriana Valio[2]
[1] Laboratory of Space Weather, NSSC/CAS, Beijing, China
[2] Center for Radio Astronomy and Astrophysics Mackenzie, Mackenzie Presbyterian University, São Paulo, Brazil; douglas93f@gmail.com
Received 2021 March 8; revised 2021 May 23; accepted 2021 May 31; published 2021 June 25

Abstract

Solar flares, resulting from magnetic activity of the Sun, are among the most energetic events in the solar system and in extreme cases directly affect our highly technological society. In this work, we analyze a solar flare detected at millimeter and centimeter wavelengths, as well as X-rays above 1 MeV. Observations of solar flares at these energy bands provide diagnostics of the energetic accelerated electrons and the magnetic fields where the emission is produced. During the SOL2013-05-13 solar flare, radio data were obtained by the telescope system POlarisation Emission of Millimeter Activity at the Sun, which observes the Sun at 45 and 90 GHz with polarization measurements, and at microwaves (1–15 GHz) by the Radio Solar Telescope Network. For the same event, X-ray emission was detected by the RHESSI and Fermi satellites. Spectra at both wavelengths were constructed and fit separately to yield the accelerated electron energy distribution that produced the emission. The optically thin radio spectral index was calculated by fitting the Ramaty model of gyrosynchrotron emission to the observed radio spectrum, whereas the hard X-ray spectral index was obtained from the spectral fit assuming a thermal emission model plus a nonthermal broken power-law distribution. Finally, both spectral indexes were compared and confirmed that the index obtained from the radio spectrum agrees with the index of the X-ray spectrum for energies above the break energy of ∼600 keV. Thus, the hard X-rays more energetic than 600 keV and high radio frequencies of solar flares are emitted by the same population of high-energy accelerated electrons. This result indicates that the accelerated electrons have an energy distribution best represented by a broken power law, with a breakup above energies around 1 MeV.

Unified Astronomy Thesaurus concepts: Stellar flares (160); X-ray transient sources (1852)

1. Introduction

Observation of solar flares at multiwavelengths are fundamental to understand the physical processes involved and to provide information about the emitting particles. Since the first observations of solar flares, the temporal profiles of the emission at microwave wavelengths and hard X-rays were seen to be very similar (Peterson & Winckler 1958). Due to this temporal similarity, it is believed that the emission at both spectral ranges originates from the same population of accelerated electrons during the event. Thus, observing the same event in X-rays and microwaves simultaneously enables the study of the energy distribution of the accelerated electrons from tens to hundreds of keV, up to hundreds of MeV. Moreover, the evolution of nonthermal electrons and their energy spectra is a valuable means of restricting the acceleration mechanisms in operation during these events.

Electrons undergo successive collisions before they loose all their suprathermal energy and emit hard X-ray photons (Lin & Hudson 1971). Thus an electron that emits a hard X-ray photon with energy E has an initial energy between 1.5 and 3 E. For the millimeter range, the energy of the emitting electrons is around MeV (White & Kundu 1992; White et al. 2011). However, the energy of the emitting electrons observed at both wavelength intervals, X-rays and millimeter, is usually different because flares are seldom observed in X-rays above 200 keV.

To our knowledge, only one study so far has analyzed simultaneous flare data at radio wavelengths and high-energy X-rays above MeV. Trottet et al. (1998) analyzed the SOL1990-06-11 electron-dominated event observed in hard X-rays up to 56 MeV and radio emission up to 50 GHz. To determine the spectral index of the microwave emitting electrons, the authors analyzed the spectral indices of hard X-ray photons for three types of electron propagation: free propagation, turbulent trapping, and perfect trapping. The authors found that the centimeter–millimeter index values from the free propagation and turbulent trapping models agreed reasonably well with the observed X-ray spectral indices. Therefore, they concluded that the centimeter–millimeter emission of this event originates from electrons with energy higher than 400–700 keV.

In this work, we analyze the solar flare SOL2013-05-13 that peaked at 16:05 UT, observed at millimeter wavelengths and hard X-rays, to study the characteristics of the accelerated electrons that produced these emissions. The observations are described in the next section, as well as the radio and X-ray spectra. Section 3 presents the electron energy distribution resulting from model fits to the data. Finally the results are discussed and the main conclusions explained in Section 4.

2. Observations and Spectra

The event SOL2013-05-13, a GOES X2.8-class event, reached maximum flux at 16:05 UT, and occurred in active region AR1748 (N11E85). This event was completely observed by the RHESSI satellite (Lin et al. 2004) that detected photons reaching energies of up to 1 MeV, while the Fermi telescope (Meegan et al. 2009) observed only the final part of the event in the 300–1000 keV range. This event occurred in the eastern limb of the Sun and is shown in Figure 1 with the Solar Dynamics Observatory/Atmospheric Imaging Assembly (SDO/AIA) UV image of the flare with the hard X-ray sources

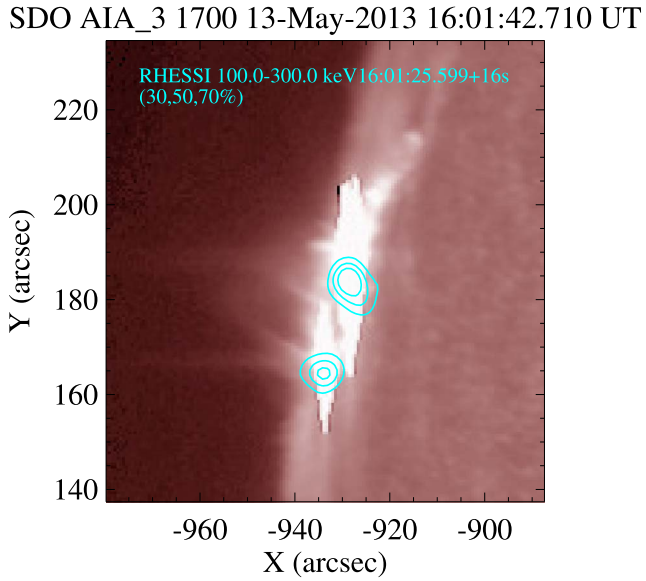

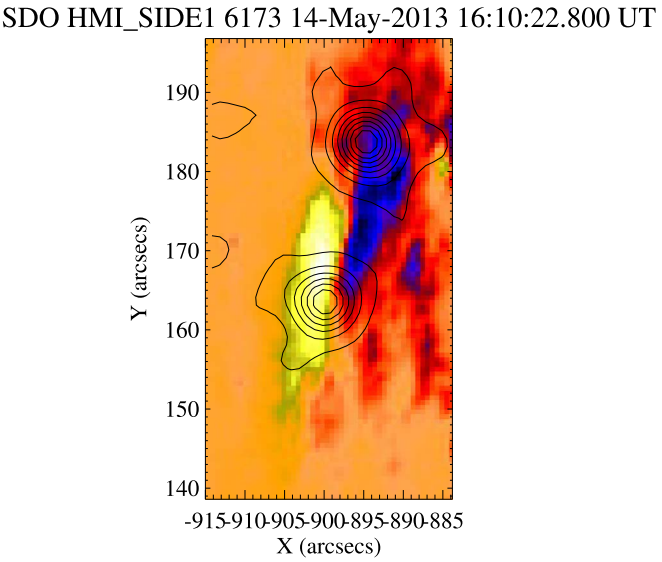

Figure 1. Image of the solar limb in 1700 Å from SDO/AIA showing the region of the solar flare near the time of the first peak. The intensity contours are 30%, 50%, and 70% of the hard X-ray RHESSI 100–300 keV emission. Helioseismic and Magnetic Imager (HMI) magnetogram of the active region one day after the SOL2013-05-13 event with RHESSI 100–300 keV source contours overlaid.

overlaid as contours. The reconstructed RHESSI hard X-ray images were obtained using the CLEAN procedure (Hurford et al. 2002) with the frontal detectors in the energy range of 100 to 300 keV. Two main sources of emission, most likely loop footpoints, were seen throughout the event.

Hard X-ray time profiles of the photon flux at 300, 400, and 500 keV observed by RHESSI are shown in the top panel of Figure 2, where four peaks can be distinguished. These four time intervals, depicted in the Figure 2 by vertical dashed lines, were defined for the accumulation of counts. The start and end times of each interval are listed in Table 1.

This same event was simultaneously observed at radio wavelengths. The 5–15 GHz microwave emission is from the Radio Solar Telescope Network (RSTN) Sagamore Hill

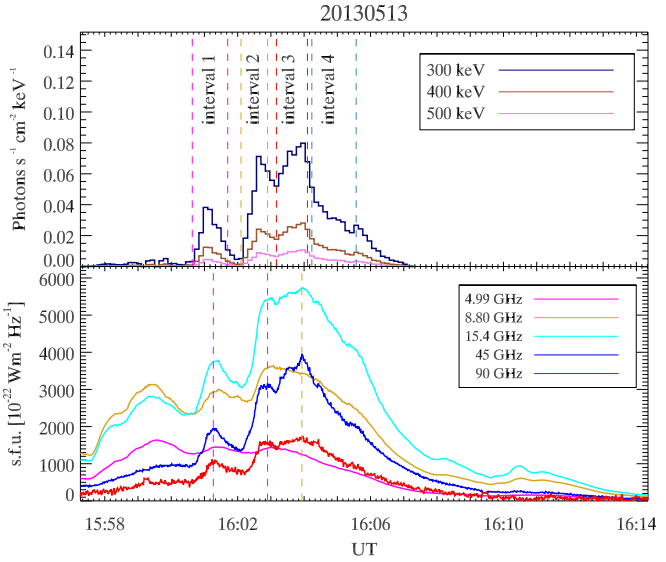

Figure 2. Temporal profiles of hard X-rays observed by RHESSI (upper panel) and at radio wavelengths from 5 to 90 GHz by POEMAS and RSTN (lower panel).

observatory with a 1 s temporal resolution, while the millimeter data were observed by the telescopes POlarization Emission of Millimeter Activity at the Sun (POEMAS) that monitor the Sun at 45 and 90 GHz with circular polarization (Valio et al. 2013). The latter telescopes are installed at the El Leoncito Astronomical Complex Observatory (CASLEO), in Argentina at 2550 m of altitude.

The temporal profiles of the microwave and millimeter emissions are shown in the bottom panel of Figure 2. The millimeter data, initially with a 10 ms temporal resolution, were integrated to 1 s time resolution and combined with the microwave data. This allowed the radio flux spectra of the flare, every 1 s, from 5 to 90 GHz to be built.

2.1. Spectrum of Hard X-Rays

The methods for processing X-ray data described in this section apply both to the Fermi and the RHESSI satellites. The Object SPectral EXecutive (OSPEX) routine was used for data retrieval, calibration, and spectral fit of the X-rays. OSPEX is a software package within Solar Software (Tolbert & Schwartz 2020) developed for treating the X-ray spectrum of space telescopes such as Fermi and RHESSI, starting from the raw data. The RHESSI data were acquired in files using the Spectral Response Matrix format and the spectrum files, both in FITS formats, as these files can be input directly into the OSPEX software.

To obtain the X-ray spectrum, a constant background is subtracted from the raw data observed by the Fermi and RHESSI missions. Afterward, the interval of interest is selected, and the data accumulated according to the intervals selected within the event. The four time intervals selected for this event are listed in Table 1. Finally, the spectrum is fitted for each accumulated interval using a two-component model: a low-energy thermal function plus a power law at higher energies.

Only the final part of the event, from 16:04:39 UT onward, was observed by both RHESSI and Fermi telescopes. The Fermi satellite detected photons with higher energies (up to 1 MeV) than the RHESSI satellite. Using this last time period,

Table 1
Hard X-Ray Four Time Intervals for Spectral Analysis

Parameters	Interval 1	Interval 2	Interval 3	Interval 4
Start time (UT)	16:00:41.6	16:02:06.4	16:03:11.6	16:04:10.8
End time (UT)	16:01:44.4	16:02:56.0	16:04:08.4	16:05:32.8
EM (10^{49} cm^{-3})	1.21 ± 0.03	1.77 ± 0.04	2.33 ± 0.05	2.45 ± 0.05
T (keV)	2.60 ± 0.01	2.64 ± 0.01	2.56 ± 0.01	2.44 ± 0.01
A_0 (ph cm^{-2} sec^{-1})	4.23 ± 0.02	6.16 ± 0.03	6.82 ± 0.03	3.11 ± 0.01
γ_1	2.90 ± 0.01	2.62 ± 0.01	2.38 ± 0.01	2.46 ± 0.01
E_1 (keV)	113 ± 11	111 ± 5	122 ± 3	118 ± 6
γ_2	3.1 ± 0.1	3.03 ± 0.03	2.99 ± 0.03	2.84 ± 0.04
E_2 (keV)	520 ± 60	530 ± 70	680 ± 120	400 ± 60
γ_3	1.2 ± 0.4	1.9 ± 0.3	1.6 ± 0.6	2.1 ± 0.1

Note. The accumulated photon spectrum for each interval was fitted by a thermal function plus a triple power law, with energy breaks, E_1 and E_2, and the energy spectral indices, γ_1, γ_2, and γ_3.

we can verify whether the part of the spectrum of highest energy observed by RHESSI agrees with the data observed by Fermi.

For this time interval, three different types of power-law fits were applied to the RHESSI hard X-ray spectrum: a single, a double, and a triple power law. These fits are shown in the three left plots of Figure 3 for the last time interval of the SOL2013-05–13 event. The same power laws were fit to the Fermi data, and are shown in the three right panels of Figure 3. The total flux of thermal plus power laws resulting from the fit are highlighted by the continuous pink line for RHESSI and the continuous blue line for Fermi, with the observed data represented by crosses. The energy range for the fit was from 216 to 1200 keV for Fermi and 10 to 1000 keV for RHESSI. As can be seen in Figure 3, the observed data are better fitted by a triple power law, for both Fermi and RHESSI observations. This best fit is corroborated by the χ^2 value given in each panel.

The results of the triple power law for both satellite data during the last time interval are shown together in Figure 4, where the Fermi BGO detector data are shown in black. As can be seen, there is an excellent correspondence of the spectra observed by both telescopes in the final stage of the event. Moreover, Fermi has detected photons at higher energies than RHESSI and, interestingly, presents harder spectral indices. The model spectral index of higher energy, above 780 keV, is 1.58.

The comparison between the spectral fit for the fourth interval of the event from both telescopes reveals that the spectral index (2.12) of the highest-energy photons above 397 keV observed by RHESSI corresponds well with the spectral index (2.33) for energies between 370 and 780 keV break energies observed by Fermi (see Figure 4). Therefore, we can trust the indices of higher-energy photons detected by RHESSI during the first three time intervals.

To obtain the photon flux in the first three intervals, we apply a model with a thermal function, $v_{\rm th}$, the template $v_{\rm ern}$, which includes the calculation of the 511 keV annihilation line in solar atmosphere conditions, and the triple power law to the RHESSI observations. The results for the break energies and photon spectral indices are listed in Table 1.

2.2. Radio Flux Density Spectrum

The radio flux density spectra were built combining the 1–15 GHz data from RSTN with the millimetric 45 and 90 GHz observations by POEMAS, every 1 s. Then the flux density spectra were fit using the Ramaty (1969) gyrosynchrotron model. The Ramaty et al. (1994) theory with homogeneous solution of the radiative transfer equation considered here had only four free parameters: (i) the magnetic field, (ii) the emitting source area, (iii) the accelerated electron density, and (iv) the spectral index of the accelerated electron energy distribution. Thus, the other parameters such as depth of the emitting source and the line-of-sight angle were considered constant in all fits, and their values were 1×10^9 cm and 84°.

The radio flux density spectrum constructed by combining the microwave and millimetric emissions in three instants of time identified by the vertical dashed lines in the lower panel of Figure 2 are plotted in Figure 5. The gyrosynchrotron model fit is shown by the blue curve, and the results of the fit are listed in Table 2: the magnetic field, emitting source size, the total number of accelerated electrons, and the spectral index, δ_r, of the accelerated electrons that produced the radio emission. As can be seen, the radio emission was produced by a small source with a radius of 24″–32″, which yields a density of accelerated electrons of about $1–10 \times 10^5$ cm^{-3}, assuming a spherical source, and is located in a region of ≈590–680 G magnetic field. Inspection of the magnetogram one day later (see Figure 1) yields magnetic fields in the range −900 to +630 within the flaring region rotated to the time of the magnetogram. We chose a magnetogram a day later due to the proximity of the limb on the time of the flare. Thus the magnetic fields inferred from the radio spectrum are compatible with photospheric values.

3. Energy Distribution of Nonthermal Electrons

As described in Section 2.1, for each time interval of the SOL2013-05-13 event, a broken power law with three spectral indices was fit to the X-ray photons depending on their energy. Here we concentrate on the two higher-energy spectral indices of the photons, γ_2 and γ_3, above ∼100 keV. The spectral index γ_2 relates to photons of energies between break energies E_1 and E_2, whereas γ_3 is for energies higher than E_2. To convert from the observed photon spectral index, γ, to spectral indices of the energy distribution of accelerated electrons, δ_X, we consider the thick target model interaction of nonthermal electrons in dense regions (Tandberg-Hanssen & Emslie 2009). For the thick target model, the spectral index δ_X is given by (Trottet et al. 1998)

$$\delta_X \approx \gamma + 1.5 \quad \text{for E} \ < 100 \text{ keV}, \tag{1}$$

$$\delta_X \approx \gamma + 1 \quad \text{for E} \geqslant 100 \text{ keV}, \tag{2}$$

depending on the energy, E, of the emitting electrons. Since the goal here is to compare this spectral index with that obtained

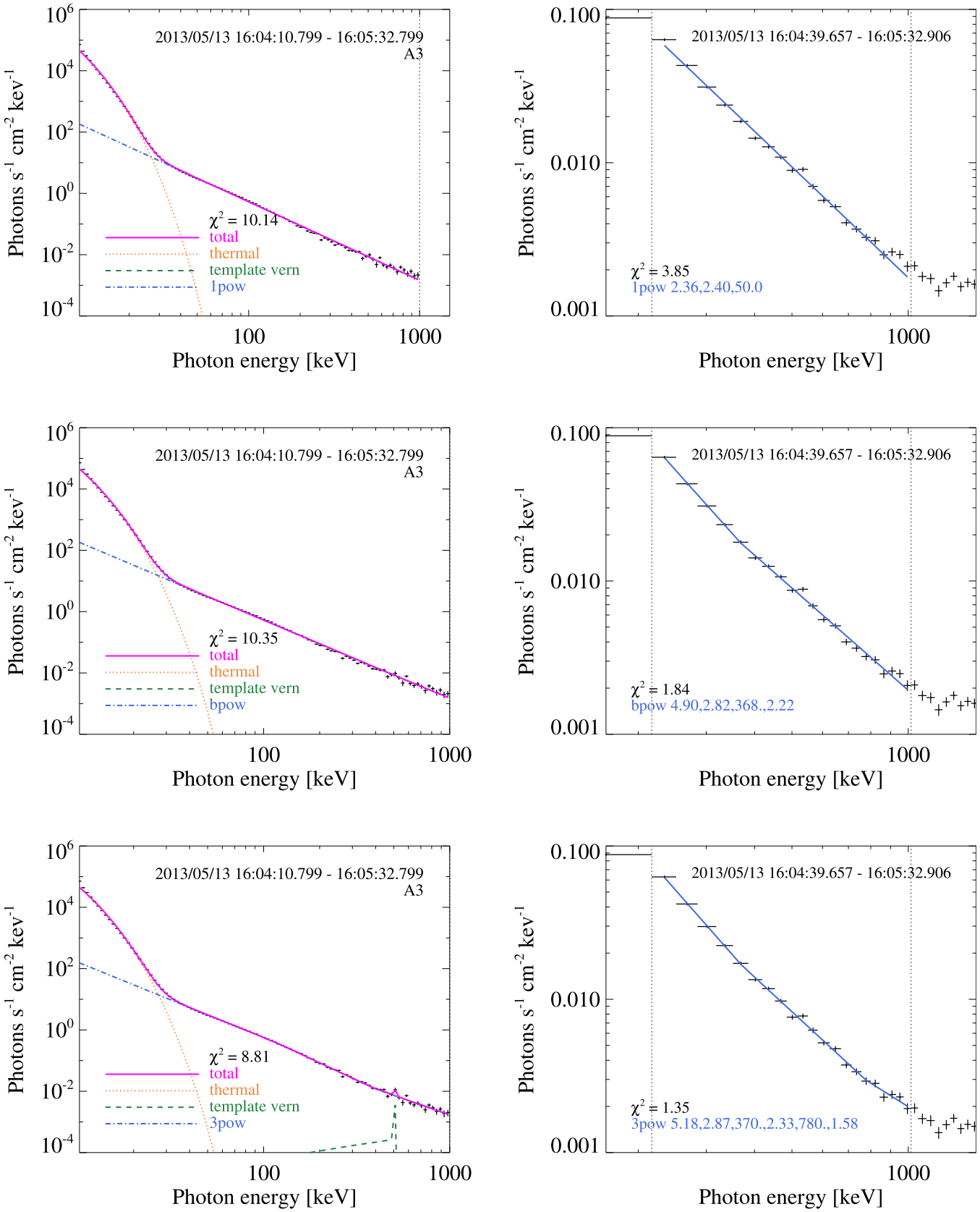

Figure 3. Hard X-ray spectra of the SOL2013-05-13 event during interval 4 observed by RHESSI (left column) and Fermi (right column). The data observed by Fermi were accumulated between 16:04:39.657 and 16:05:32.906 UT, while for RHESSI data were accumulated between 16:04:10.657 and 16:05:39.657 UT. These spectra were fit by a thermal model plus three different power laws: a single (top panels), a double (middle panels), and a triple (bottom panels) power law.

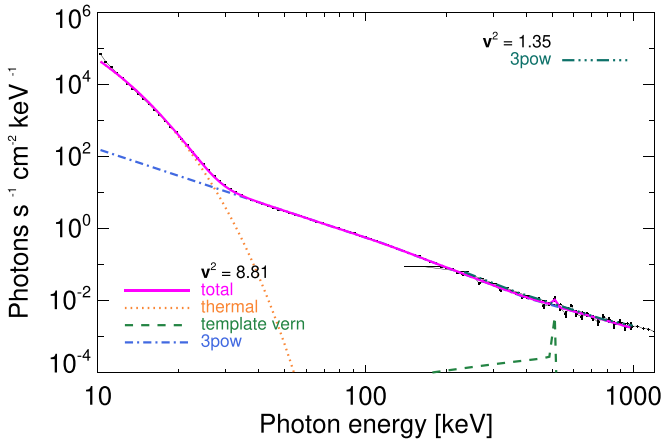

Figure 4. A comparison of the photon flux spectra per keV observed by RHESSI and Fermi telescopes (black curve) during the final phase of the SOL2013-05-13 event.

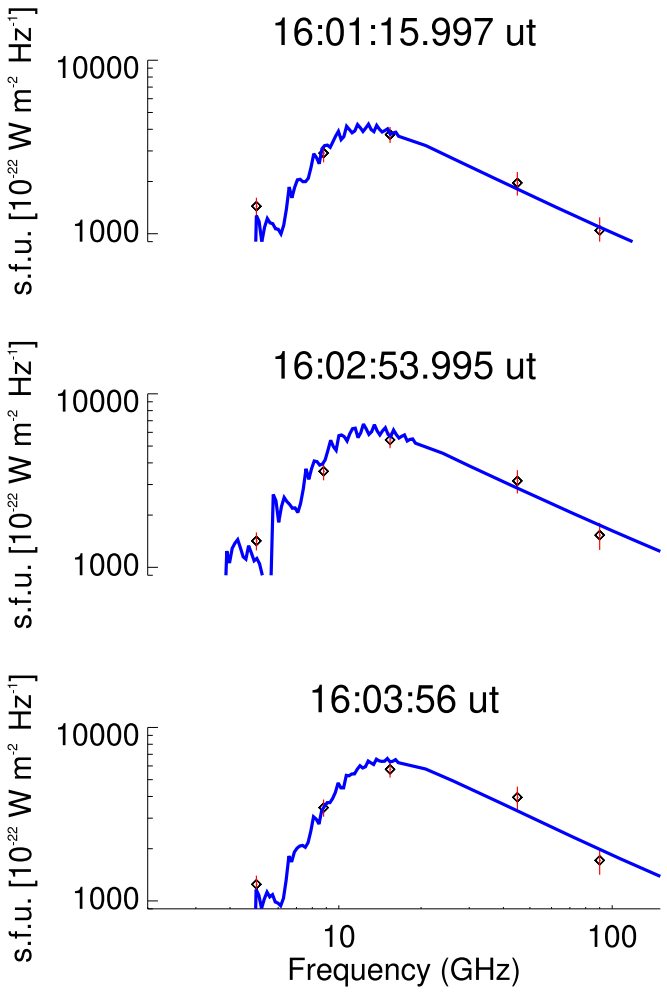

Figure 5. Examples of a radio emission spectrum and corresponding gyrosynchrotron fits for the three time intervals depicted in the bottom panel of Figure 2.

from the radio observations, we concentrate on the electrons with energy greater than 100 keV. This relation is valid for both the free propagation and turbulent trapping models considered by Trottet et al. (1998). In the free propagation model, as the name implies, the electrons freely propagate along the magnetic field producing the thick target hard X-rays whereas the radio emission is produced by the same electrons in a source above the hard X-ray emitting source. On the other hand, in the turbulent precipitation model, the electrons are trapped at the top of the magnetic loop where the radio emission is then produced.

Table 2
Results of the Fit to the Radio and Hard X-Ray Spectra

	Interval 1	Interval 2	Interval 3
Radio Spectral Parameters			
B (G)	591 ± 9	680 ± 60	589 ± 5
Radius (Arcsec)	25 ± 3	32 ± 2	23.4 ± 0.8
N_e (10^{32})	10 ± 1	11 ± 1	20 ± 2
δ_r	2.1 ± 0.1	2.1 ± 0.1	2.1 ± 0.1
Hard X-Rays ($\geqslant$100 keV)			
δ_X ($\leqslant E_2$)	4.1 ± 0.1	4.03 ± 0.03	3.99 ± 0.03
δ_X ($\geqslant E_2$)	2.2 ± 0.4	2.9 ± 0.3	2.6 ± 0.6

Note. The radio spectra were fit by the gyrosynchrotron model, whereas the free propagation and turbulent precipitation models were applied to the spectral indexes of the energy distribution of the X-ray photons.

The two bottom lines of Table 2 list the results of the spectral indices of the accelerated electrons, δ_X, derived from the spectral indices of the X-ray photons, γ_2 and γ_3, below and above E_2, respectively, obtained from Equations (1) and (2).

From the fits to the X-ray and radio spectra, the energy distribution of the accelerated electrons may be reconstructed. A comparison of the spectral index $\delta_X(\geqslant E_2)$ and δ_r from Table 2 shows a good agreement, especially for the first interval. Except for interval 2, $\delta_r \approx \delta_X$, within the uncertainty for hard X-ray photons with energies above E_2, which is around 400–700 keV (see Table 1). These photons were probably produced by electrons with energies in the range of 600–2000 keV (White et al. 2011).

The spectra of the accelerated electrons, $dN(E)/dE \propto E^{-\delta}$, in this flare can be reconstructed from the hard X-rays (Tandberg-Hanssen & Emslie 2009):

$$\frac{dN(E)}{dE} = 3.04 \times 10^{24} \frac{A_i B(\Gamma) L}{E_i^{1.5}} \left(\frac{E}{E_i}\right)^{-\delta_X} \text{electrons/KeV}, \quad (3)$$

where A_i, E_i, and $\delta_x = \gamma_i + c$ are the normalization constant, break energy, and the photon spectral index, respectively, listed in Table 1 for each of the three energy intervals of the triple power law. The constant c is either 1.5 or 1.0 depending on the energy of the electrons, according to Equations (1) and (2). E_0 is the low-energy cutoff assumed to be 10 keV and $B(\Gamma) = \Gamma^2(\Gamma - 1)^2\beta(\Gamma - 0.5, 1.5)$, where $\beta(x, y)$ is the beta function. The resulting $B(\Gamma)$ is a function with values between 10–60 (here we adopted a value of 40), and L is the source depth taken as 1×10^9 cm. The energy distribution of the hard X-ray emitting electrons is depicted in Figure 6 as the broken black line, for the three time intervals considered.

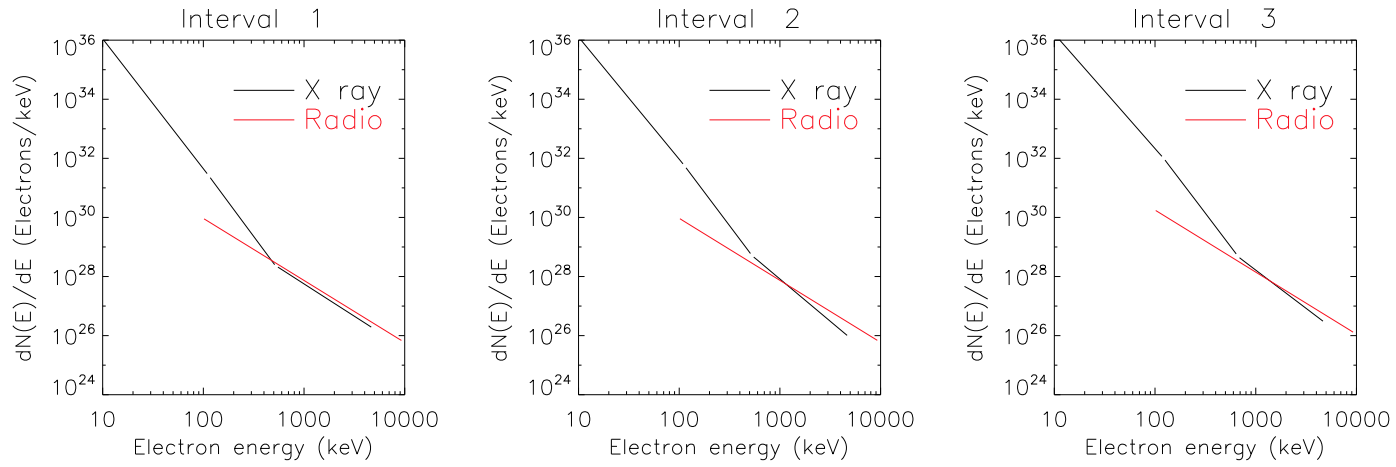

Figure 6. Broken power-law spectrum of the accelerated electron energy distribution.

On the other hand, the energy distribution of the radio emitting electrons is estimated from

$$\frac{dN(E)}{dE} = (\delta - 1)E_0^{\delta-1}N_e\ E^{-\delta_r} \quad \text{electrons/KeV}, \qquad (4)$$

where N_e is the total number of electrons and δ_r is the spectral index listed on Table 2. This function is shown in Figure 6 as a red line.

4. Discussion and Conclusion

The solar flare SOL2013-05-13 that occurred at the eastern limb of the Sun was simultaneously observed at millimeter wavelengths by the POEMAS polarimeter system (at 45 and 90 GHz), microwaves by RSTN (1–15 GHz), and in hard X-rays by RHESSI and Fermi space telescopes. The RHESSI telescope observed the entire event while Fermi detected only the final part. A good agreement was found between the spectral indices of the high-energy photon spectra, during the fraction of time observed simultaneously by both X-ray telescopes (see Figure 4), thus confirming the spectral fits of the first three time intervals (intervals 1, 2, and 3) observed only by RHESSI.

The spectra at both wavelength regimes were constructed and fit by a nonthermal energetic electron population independently during three time intervals throughout the flare. The radio spectra were fit by the gyrosynchrotron model of Ramaty (1969), whereas the hard X-ray photon spectra were fit by a thermal component plus a triple power law. Hard X-ray spectra presented in this work were seen to have at least two breaks in energy. The first one at around 100 keV, and a second one above 400–700 keV.

The energy distribution spectral index, δ_X, of the hard X-ray emitting electrons was computed assuming thick target emission. Moreover, only electrons with energy higher than 100 keV were considered for comparison with the radio data. On the other hand, the spectral index, δ_r, of the energy distribution of the radio emitting electrons is an output of the Ramaty (1969) model fit to the radio spectra. Both spectral indices are listed on Table 2. As can be seen from these results, the spectral indices of the energy distribution of the radio emitting electrons agree reasonably well with that of the hard X-ray producing electrons, when considering photons with energies higher than 400–700 keV or, conversely, electrons with energies $\geqslant$1 MeV.

The reconstructed energy spectra of the accelerated electrons can be represented by a broken power law with break energy around 500 keV, and spectral index $\delta = 4$ below this energy and $\delta = 2$ above (see Figure 6). The photons detected below energies of ~500 keV (representing E_2) are produced by lower-energy electrons with an energy distribution index of $\delta \approx 4$, whereas the higher-energy hard X-rays and radio emission (microwaves and millimeter waves) are generated by electrons with energies $\geqslant$1 MeV and $\delta \approx 2$.

Previous works, such as Silva et al. (2000), showed that the spectral indices for the population of accelerated electrons emitting the radio and the X-rays do not match, with the radio index being harder than that of the X-rays by approximately 2 units. The authors explained this discrepancy by the fact that the radio emission is produced by higher-energy electrons than the X-rays, and that the common accelerated electron population has a power-law energy distribution that breaks up above 300 KeV. Since the hard X-rays analyzed in Silva et al. (2000) had energies lower than ~200 keV, the results are in agreement with those presented here for the SOL2013-05-13 flare, as well as the two discrepancies in the spectral indices of hard X-rays and radio.

Moreover, Vestrand (1988) and Dennis (1988) report giant flares observed in hard X-rays with energies larger than 1 MeV that showed a breakup in their photon spectra at ~300 keV. More recently, from the analysis of an X8.2 solar flare detected in hard X-rays by RHESSI, Ning et al. (2019) found a broken-up power-law spectra originating from a coronal source. However, the break energy was only about 50 keV and the harder spectral photon index was ~3.

There are basically three possible explanations for electrons to exhibit such a broken-up power-law energy distribution. The first is that there are two components, or sources, of energetic electrons that were produced by two different acceleration mechanisms (Silva et al. 2000; Krucker et al. 2008). However, to produce a similar temporal evolution in radio and hard X-ray emission, there must be a close link between these two acceleration mechanisms. Alternatively, the second possibility is that the difference in spectral indices is due to physical characteristics of a certain acceleration mechanism and/or a transport process of electrons such as diffusive shock acceleration (Li et al. 2013), where a hardening of the spectrum occurs around 500–600 keV, or stochastic acceleration due to wave–particle interactions in the presence of Coulomb collisions (Hamilton & Petrosian 1992). Yet another explanation for the hardening of the spectra is the trap-plus-precipitation model (Lee & Gary 2000) in which the electrons with lower energy escape from the trap due to Coulomb collisions leaving the higher-energy electrons trapped in the loop

top. The SOL2013-05-13 event studied here simultaneously presented hard X-ray emitting electrons above 400–700 keV as well as emitting electrons in the millimeter range, believed to have energies larger than MeV. This solar flare and the event observed by Trottet et al. (1998) are the only ones so far presenting simultaneous detection of hard X-rays of energies higher than 500 keV and the corresponding electrons emitting in the millimeter range. In both cases when energetic enough hard X-rays are detected, the spectral indices match the harder index of electron energy distribution inferred from radio observations.

The authors would like to thank the anonymous referee for insightful suggestions that much improved the manuscript. We acknowledge the Brazilian funding agencies FAPESP (grants #09/50637-0, #13/24155-3, and #13/10559-5) and Mack-Pesquisa for partial funding of this work. D.F.S. acknowledges a CAPES PhD fellowship and thanks the China-Brazil Joint Laboratory for Space Weather (CBJLSW).

ORCID iDs

Douglas Félix da Silva https://orcid.org/0000-0001-5204-0467
Adriana Valio https://orcid.org/0000-0002-1671-8370

References

Dennis, B. R. 1988, SoPh, 118, 49
Hamilton, R. J., & Petrosian, V. 1992, ApJ, 398, 350
Hurford, G. J., Schmahl, E. J., Schwartz, R. A., et al. 2002, SoPh, 210, 61
Krucker, S., Hurford, G. J., MacKinnon, A. L., Shih, A. Y., & Lin, R. P. 2008, ApJL, 678, L63
Lee, J., & Gary, D. E. 2000, ApJ, 543, 457
Li, G., Kong, X., Zank, G., & Chen, Y. 2013, ApJ, 769, 22
Lin, R. P., Dennis, B., Hurford, G., Smith, D. M., & Zehnder, A. 2004, Proc. SPIE, 5171, 38
Lin, R. P., & Hudson, H. S. 1971, SoPh, 17, 412
Meegan, C., Lichti, G., Bhat, P. N., et al. 2009, ApJ, 702, 791
Ning, H., Chen, Y., Lee, J., et al. 2019, RAA, 19, 173
Peterson, L., & Winckler, J. R. 1958, PhRvL, 1, 205
Ramaty, R. 1969, ApJ, 158, 753
Ramaty, R., Schwartz, R. A., Enome, S., & Nakajima, H. 1994, ApJ, 436, 941
Silva, A. V. R., Wang, H., & Gary, D. E. 2000, ApJ, 545, 1116
Tandberg-Hanssen, E., & Emslie, A. G. 2009, The Physics of Solar Flares (Cambridge: Cambridge Univ. Press)
Tolbert, K., & Schwartz, R. 2020, OSPEX: Object Spectral Executive, ascl:2007.018
Trottet, G., Vilmer, N., Barat, C., et al. 1998, A&A, 334, 1099
Valio, A., Kaufmann, P., Giménez de Castro, C. G., et al. 2013, SoPh, 283, 651
Vestrand, W. T. 1988, SoPh, 118, 95
White, S. M., Benz, A. O., Christe, S., et al. 2011, SSRv, 159, 225
White, S. M., & Kundu, M. R. 1992, SoPh, 141, 347